Designing a template bank to observe compact binary coalescences in Advanced LIGO's second observing run

Tito Dal Canton[1, 2, *] and Ian W. Harry[3, †]

[1] *Max Planck Institute for Gravitational Physics (Albert Einstein Institute), Callinstrasse 38, D-30167 Hannover, Germany*
[2] *NASA Postdoctoral Program Fellow, Goddard Space Flight Center, Greenbelt, MD 20771, USA*
[3] *Max Planck Institute for Gravitational Physics (Albert Einstein Institute), Am Mühlenberg 1, D-14476 Potsdam-Golm, Germany*

(Dated: May 4, 2017)

We describe the methodology and novel techniques used to construct a set of waveforms, or template bank, applicable to searches for compact binary coalescences in Advanced LIGO's second observing run. This template bank is suitable for observing systems composed of two neutron stars, two black holes, or a neutron star and a black hole. The Post-Newtonian formulation is used to model waveforms with total mass less than 4 $M_\odot$ and the most recent effective-one-body model, calibrated to numerical relativity to include the merger and ringdown, is used for total masses greater than 4 $M_\odot$. The effects of spin precession, matter, orbital eccentricity and radiation modes beyond the quadrupole are neglected. In contrast to the template bank used to search for compact binary mergers in Advanced LIGO's first observing run, here we are including binary-black-hole systems with total mass up to several hundreds of solar masses, thereby improving the ability to observe such systems. We introduce a technique to vary the starting frequency of waveform filters so that our bank can simultaneously contain binary-neutron-star and high-mass binary-black hole waveforms. We also introduce a lower-bound on the filter waveform length, to exclude very short-duration, high-mass templates whose sensitivity is strongly reduced by the characteristics and performance of the interferometers.

I. INTRODUCTION

Merging binary systems composed of stellar-mass compact objects are a primary source of gravitational-wave (GW) signals in ground-based interferometers such as Advanced LIGO [1, 2], Advanced Virgo [3] and Kagra [4, 5]. The first observing run of Advanced LIGO (O1) yielded two binary-black-hole (BBH) observations with $> 5\sigma$ signficance, GW150914 and GW151226 and one further observation with $\sim 2\sigma$ significance, LVT151012 [6–8]. Many additional observations are expected in the coming years [8].

The most sensitive search for compact binary mergers leverages accurate physical models describing the dynamics of such systems and their associated GW signals. The search parameter space, typically composed of the masses and spin parameters of the components of the binary, is covered by a discrete grid of model waveforms called a *template bank* [9–15]. Detector data are then correlated (or matched-filtered) with each waveform in the bank, producing a list of *triggers*, which are defined by local maxima of the matched-filter signal-to-noise ratio (SNR) being larger than a certain threshold [16]. Each trigger is tagged with a variety of parameters including the originating template, the time of merger and a single-detector ranking statistic based on the SNR. Triggers in coincidence between different detectors are further ranked according to a network statistic and finally assigned a statistical significance based on empirical background distributions. Three independently implemented pipelines are currently using such methods to search for compact binary mergers in Advanced LIGO data: `PyCBC` [17–20], `GstLAL` [21–23] and `MBTA` [24].

A number of variables are used in the construction of a template bank: (i) the parameter space to search over (range of masses and spin parameters of the merging objects), (ii) the power spectral density of the detector noise, (iii) the particular waveform model(s) to use, (iv) the maximum fractional loss in sensitive range due to the discrete coverage of the search space with a finite number of templates and (v) the starting frequency of template waveforms. These choices impact both the sensitivity of the search as well as its computational cost [25].

The all-sky, blind, template-based search for stellar-mass compact binaries in O1 employed a template bank with a maximum total mass of $100M_\odot$ [8, 26]. A second all-sky blind search targeted BBH systems with larger masses ($50M_\odot$ to $600M_\odot$) and employed independently-constructed template banks for the `gstlal` and `PyCBC` analyses [27]. The basic search technology employed for the two searches, however, remained the same. In Advanced LIGO's second observing run (O2), it is desired to combine these two parameter spaces together into a single search. In fact, separate and partially-overlapping searches require artificial boundaries across the continuous parameter space of compact binary systems. Calculating the statistical significance of candidate events is also more complicated, as it requires accounting for the same event being detected by multiple searches as well as accounting for the relative sensitivities of the involved searches [28]. Therefore, covering the largest possible parameter space in a single search is more straightforward.

* tito.canton@ligo.org
† ian.harry@ligo.org

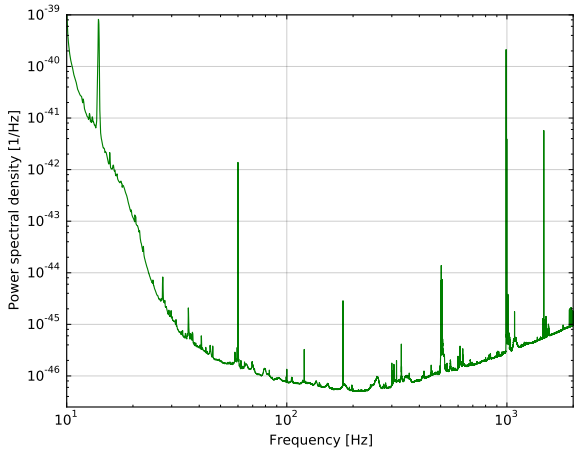

FIG. 1. Power spectral density used to model the detector noise in the construction of the bank. The curve is the harmonic mean of the power spectral densities measured at the Hanford and Livingston detectors.

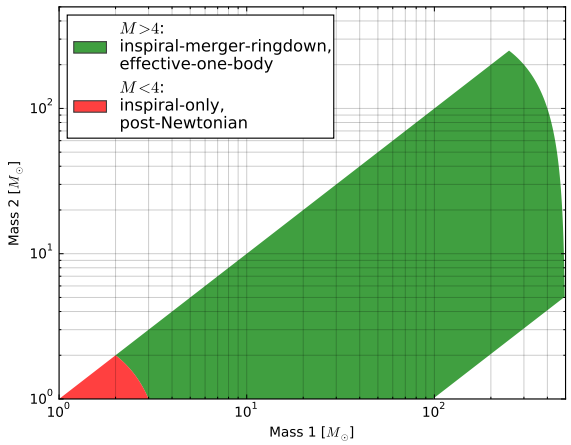

FIG. 2. Variation of the template waveform model used to cover the search parameter space.

Here we describe a template bank resulting from this decision, whose construction involves a number of novel developments. Such a bank is currently being used by the `PyCBC` pipeline to search for compact binary mergers in Advanced LIGO's O2 data.

The paper is organized as follows. Section II describes our choice of model for the template waveforms, the extent of the search parameter space, our criterion for defining a variable template starting frequency, the placement of templates and the characteristics of the resulting bank. In section III we demonstrate the ability of the bank to recover signals. We summarize our conclusions in section IV. Throughout the paper, the heavier and lighter objects of a compact binary have masses m_1 and m_2 and dimensionless spin components along the orbital angular momentum χ_1 and χ_2. The binary's total mass and mass ratio are referred to as $M = m_1 + m_2$ and $q = m_1/m_2$. Masses are taken to be in the detector frame, i.e. redshifted.

II. DESIGN AND CONSTRUCTION

A. Noise spectral density

The noise power spectral density used for constructing the bank (figure 1) is calculated as the harmonic mean of the power spectral densities from the Hanford and Livingston detectors, following [29]. Averaged single-detector power-spectral densities are estimated from a week of engineering data acquired immediately before the start of Advanced LIGO's second observing run following methods described in [16, 18].

B. Waveform models

The template bank used to analyse O1 data used a reduced-order model [30] of the aligned-spin effective-one-body waveform model described in [31] for templates with total mass $M \geq 4M_\odot$. For $M < 4M_\odot$ the merger and ringdown portions of the waveform contain a negligible amount of power relative to the inspiral, so a frequency-domain post-Newtonian inspiral-only model was used instead, due to simplicity and reduced computational cost [32]. The post-Newtonian model included orbital terms up to 3.5PN order [32], and spin-related corrections up to 2.5PN order [33]. It imposed a termination of the waveform at the frequency of the innermost stable circular orbit of two Schwarzschild black holes (BHs) with total mass M.

Following recent development, for the O2 template bank a newer version of the effective-one-body waveform model is used [34]. The new model is calibrated to a larger set of numerical-relativity results, which improve it especially for high mass ratios and high spin magnitudes. We choose to continue using the frequency-domain post-Newtonian inspiral-only model for $M < 4M_\odot$, but the model is updated to include spin effects up to 3.5PN order [35]. The regions of searched mass space covered by different waveform models are visualized in figure 2. All waveform models described in this section, and used in this work, are freely accessible in the `lalsimulation` package [36][1].

[1] The internal `lalsimulation` names for the waveform models described here are `SEOBNRv2` and `SEOBNRv2_ROM_DoubleSpin` for the effective-one-body model used in the O1 template bank and its reduced-order representation. `SEOBNRv4` and `SEOBNRv4_ROM` denote the improved effective-one-body model and reduced-order representation used in the O2 template bank. `TaylorF2` is the

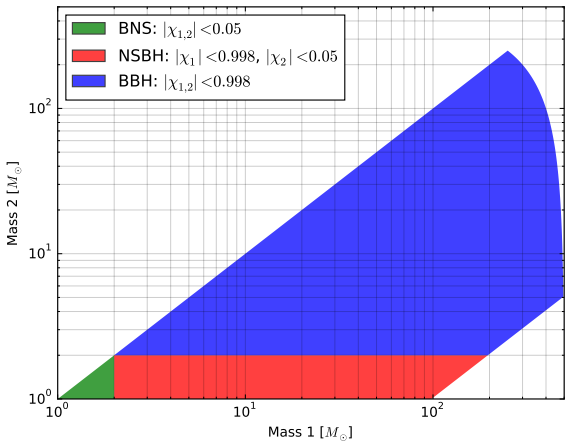

FIG. 3. Projection of the O2 search parameter space in the plane of the component masses. Colors indicate regions associated with different spin limits on the components.

C. Parameter space

The lower bound on the template bank mass space is a limit on component masses, specifically that the masses of both components are restricted to be larger than $1M_\odot$, matching what was used in O1. Lowering the component masses even further would rapidly increase the number of templates, and sub-$M_\odot$ templates would only be sensitive up to a few tens of megaparsecs, while there is little expectation of NSs with sub-$M_\odot$ masses [37]. The mass ratio in O1 was limited to $q \lesssim 98$ as this was the upper limit for which the effective-one-body waveforms were available. The same limit exists for the improved model that is used for the O2 template bank. The high-mass boundary in O1 was simply given as $M < 100M_\odot$. In O2 we increase the limit on total mass to $M < 500M_\odot$, therefore including most of the mass range covered by the O1 search targeting intermediate-mass BBH [27]. As done in O1, components with mass below $2M_\odot$ are assumed to be NSs and are assigned dimensionless aligned-spin parameters restricted to spin magnitude < 0.05. This enables the search to detect NSs with spins up to 0.4 [38] corresponding to the fastest-spinning known pulsar [39]. Heavier components, likely to be BHs, are given spins between ± 0.998 to account for the large spins observed in X-ray binaries [40]. This is slightly larger than the O1 range (± 0.9895) thanks to the increase of possible spin values in the improved effective-one-body waveform model. The boundaries of the search space are shown in figure 3.

Extending the mass range is not as simple as raising the maximum total mass, however. Because of the wide range of mass ratios and spins, high-mass waveforms have a large variety of time-frequency structure. Waveforms associated with large mass ratios and high aligned spins complete many cycles in the LIGO sensitive band, last for a relatively long time and coalesce at relatively large frequency. Those associated with high *antialigned* spins, instead, merge at or below the lowest sensitive frequency (~ 20 Hz) and complete only a few cycles in band, producing a much shorter signal. It has been found empirically that in the `PyCBC` search technique, it is difficult to distinguish if triggers produced by such short-duration templates are due to instrumental artifacts or due to astrophysical GW signals [20, 41]. Given their short time scales, such signals would also be efficiently detected by generic transient-GW searches (see e.g. [42]) and therefore are not a high priority target compared to other regions of the parameter space.

In light of the above considerations we calculate the duration of each waveform in the time domain and impose a boundary on the parameter space that all waveforms must have a duration greater than 150 ms. For post-Newtonian templates, the duration is defined as the usual chirp time [43]. For effective-one-body templates, it is defined as the time taken by the waveform to go from the starting frequency to the ringdown frequency [44]. The latter definition is increased by 10% in order to account for potentially long ringdowns. The value of 150 ms is chosen empirically based on the observed variation of the background distribution in engineering data. This translates to an irregularly-shaped high-mass boundary for the bank, which varies with the total mass, the mass ratio and the spin parameters. The maximum total mass for equal-mass, weakly-spinning templates is $100M_\odot$ while high-mass-ratio, high-aligned-spin templates still have a duration greater than 150 ms at the hard limit of $M = 500M_\odot$ (figure 4).

Further extension of the search space with currently-available waveform models is challenging. As shown in figure 4, increasing the maximum total mass above $500M_\odot$ only adds a small extra portion of parameter space, given the O2 noise curve. The currently available reduced-order model of the effective-one-body waveforms is also limited to $M \lesssim 500M_\odot$. Extending the component dimensionless spins up to the Kerr limit (± 1) is possible with the latest effective-one-body waveform model. However, as described in [45], waveforms with nearly-extremal spins can terminate with quasi-monochromatic features lasting for many cycles, depending on the mass parameters. Such features in the waveform greatly reduce the effectiveness of the signal-based consistency tests used in the `PyCBC` search method [46, 47]. This effect can potentially reduce the sensitivity of the search in regions of the parameter space where waveforms have a similar duration to such extreme-spin templates. Therefore, extending the BH spin range all the way to the Kerr limit requires further investigation of this effect, tests of the reliability of the waveform models at nearly-extremal spins and potentially the development of new

name of the post-Newtonian waveform model, as described with that name in [32].

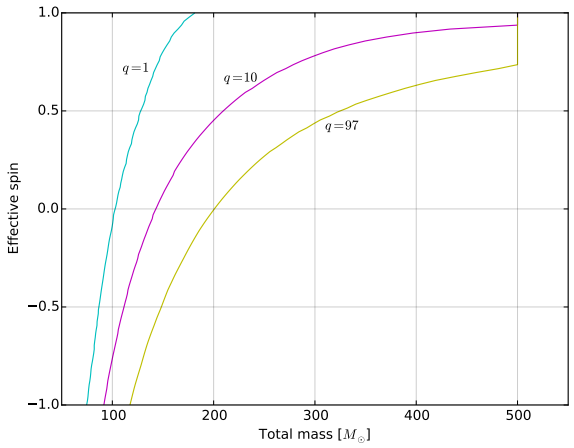

FIG. 4. High-mass boundary of the search parameter space as determined by the minimum requirement on waveform duration of 150 ms. The boundary is a curved surface, spanning a range of total masses, mass ratios and aligned-spin components (only the equal-spin case is shown here). The total mass has a hard limit at $500M_\odot$.

signal-based consistency tests applicable for such waveforms.

D. Template starting frequency

The starting frequency of template waveforms when the bank is constructed and the lower bound of the matched-filter integral over frequency [16] are in principle different parameters of the pipeline. However, we argue that using inconsistent frequencies might reduce either the effectualness of the bank or the computational efficiency of the search. Here we assume that both parameters are fixed to the same frequency $f_{\rm low}$.

The choice of $f_{\rm low}$ is then a balance of practical considerations. Reducing $f_{\rm low}$ has both beneficial and detrimental consequences depending on which region of the parameter space is being considered. A lower value of $f_{\rm low}$ equates to an increase in the sensitivity of the search, assuming Gaussian, well-calibrated noise, as more of the signal power is recovered by the matched-filter. The amount by which the sensitivity increases depends on the noise spectral density and on the template parameters, however. Below $\sim$ 20 Hz the power spectral density of the detector noise $S(f)$ increases steeply (figure 1) and the calibration of the detectors itself becomes less reliable [48]. When the template terminates at kilohertz frequencies, such as is the case for binary neutron stars (BNS) and low-mass neutron-star–black-holes (NSBH), the increase in sensitivity introduced by reducing $f_{\rm low}$ will be small. When the merger happens at tens of Hz, such as for BBH systems with a total mass of several hundred solar masses, the increase will be larger. Reducing $f_{\rm low}$ also increases the duration of template waveforms. Templates lasting hundreds of seconds introduce technical complications in the implementation of the matched filter, and are more likely to encounter an instrumental artifact within their duration, increasing the false-alarm rate or the chance of contaminating an astrophysical signal [49]. For high-mass BBH waveforms, however, the waveform duration with $f_{\rm low} = 20$ Hz will not be more than several seconds, and therefore the chance of intersecting an instrumental artifact is much lower than for longer BNS waveforms. Finally, lowering $f_{\rm low}$ also generally increases the number of required templates and thus the computational cost of the search, but it will be shown later that this is not an issue.

Previous matched-filter searches used a fixed $f_{\rm low}$ for the entire template bank. For instance, initial-LIGO stellar-mass searches used $f_{\rm low} = 40$ Hz. Following improvements in the sensitivity and calibration at low frequency, $f_{\rm low}$ was reduced to 30 Hz for the O1 search described in [8], and was set even lower when searching for BBHs with total masses up to $600M_\odot$ in [27].

The above considerations suggest that wide-mass-range template banks will benefit from a $f_{\rm low}$ that varies over the parameter space, being larger for low-mass waveforms and smaller for higher-mass ones, effectively becoming a property of each waveform in the template bank. The criterion we adopt for choosing $f_{\rm low}$ for each template waveform is the following:

$$\frac{R(f_{\rm low})}{R(15\ {\rm Hz})} = 0.995 \tag{1}$$

where

$$R(f) = \left(\int_f^{f_{\rm high}} \frac{|\tilde{h}(\nu)|^2}{S(\nu)} {\rm d}\nu \right)^{1/2} \tag{2}$$

and $\tilde{h}(\nu)$ is the template waveform in the frequency domain and $f_{\rm high}$ a frequency above which the template has a negligible amount of observable power (e.g. the Nyquist frequency). $R(f)$ is proportional to the sensitive distance of the template calculated using f as the low-frequency cutoff. Therefore, choosing $f_{\rm low}$ as in equation (1) means fixing the loss of range (0.5%) with respect to an ideal situation where data can be analyzed down to 15 Hz. This criterion is inspired by the traditional choice of determining the minimum match of the bank based on a fixed loss of range with respect to an infinitely dense bank. The reference frequency of 15 Hz is chosen to be lower than the minimum frequency used so far in a `PyCBC` analysis (20 Hz) but still well above the corner frequency of the high-pass filters used in conditioning the data for estimating the noise spectral density (10 Hz). Templates which accumulate the bulk of their range at relatively high frequency, i.e. BNS and low-mass NSBH, are automatically assigned a large $f_{\rm low}$. On the other hand, templates which coalesce at tens of Hz, such as equal-mass BBH with $M \gtrsim 100M_\odot$ or unequal-mass BBH with antialigned spins, can only satisfy equation (1) if $f_{\rm low}$ is not much larger than the reference frequency of 15 Hz.

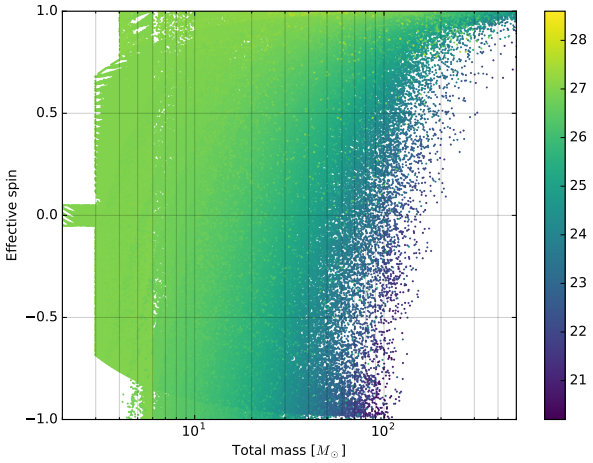

FIG. 5. Variation of the low-frequency cutoff assigned to a template across the search space. Low-mass templates sweep through the whole sensitive band of LIGO and are assigned a lower cutoff at $\sim$ 27 Hz. As we go towards the high-mass end, templates terminate at progressively lower frequencies and their cutoff drops accordingly.

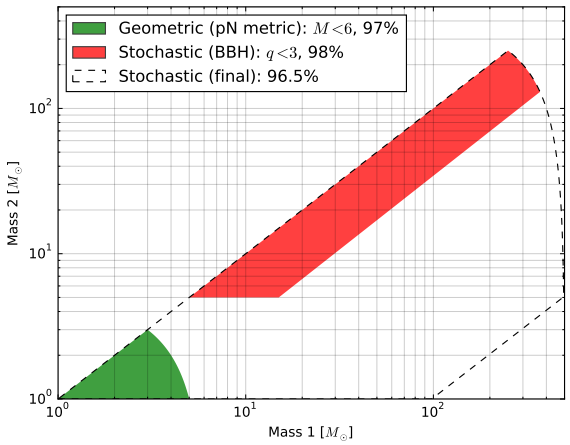

FIG. 6. Template placement methods used in covering the full parameter space.

The obtained variation of $f_{\rm low}$ across the total-mass and effective-spin space is shown in figure 5. For the lowest-mass templates $f_{\rm low} = 27$ Hz, close to the fixed value of 30 Hz manually chosen for the O1 bank. The smallest $f_{\rm low}$ is 20 Hz and corresponds to the highest-mass templates (at a fixed value of effective spin), which only have a negligible amount of power at frequencies larger than tens of Hz.

It is important to note that the variable $f_{\rm low}$ indirectly affects the high-mass boundary of the bank, because the duration of a particular waveform is calculated starting from the $f_{\rm low}$ assigned to it. This implies that an improvement in low-frequency sensitivity, combined with a fixed minimum template duration, automatically translates to a wider searched mass range. In other words, the search space naturally adapts to the evolution of the low-frequency performance of the detectors.

E. Template placement

Templates are placed using the hybrid geometric-stochastic approach described in [50] with some modifications. First, the lowest-mass region of the search space is covered via geometric placement of post-Newtonian waveform templates, using a minimum match of 97%. At the same time, the high-mass region with mass ratio less than 3 (i.e. containing the BBH signals detected thus far) is filled via stochastic placement using effective-one-body waveform templates. Since this region has yielded BBH detections before, we place templates densely here, with a minimum match of 98%. The extra coverage slightly increases the chance of detecting more BBH signals, but it only adds a small number of templates in comparison to the size of the entire bank. We combine together these two initial template banks and then "fill in" the remaining parameter space with a third stochastic placement step using effective-one-body waveform templates and a smaller minimum match of 96.5%. The different placement steps are illustrated in figure 6.

One caveat of the initial geometric placement of post-Newtonian templates is that it must assume fixed frequency limits for computing the parameter-space metric, so it cannot use a variable $f_{\rm low}$ as described in section II D. However, in the entire region covered by geometric placement, equation (1) gives $f_{\rm low} \approx 27$ Hz to a good approximation. Therefore we adopt 27 Hz as the $f_{\rm low}$ of all templates placed geometrically, as well as for calculating the metric required for geometric placement. Stochastic placement, on the other hand, simply computes the match between templates and thus automatically uses whatever $f_{\rm low}$ is assigned to each template.

F. Template bank size and structure

Creating a template bank to cover the parameter space described above and using the discussed methodology results in 4×10^5 templates, 60% larger than the bank used in O1. The additional computational cost of the pipeline due to the increased bank size is sufficiently small to not represent a limitation. The distribution of templates is shown in figure 7. The majority of templates use the effective-one-body, inspiral-merger-ringdown waveform model and only 7.5×10^4 templates, 19% of the bank, are below the $4M_\odot$ boundary and use post-Newtonian inspiral-only waveforms. The extra mass space included with respect to the O1 bank ($M > 100M_\odot$) contains 1.7×10^4 templates, 4.3% of the bank.

The "stripe" in template distribution at masses larger

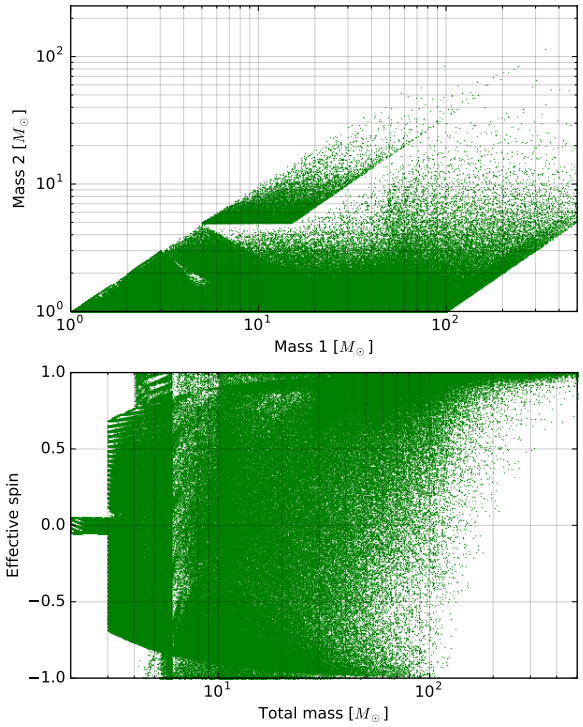

FIG. 7. Distribution of templates in two projections of the search space. The top panel shows the effect of the different placement steps (compare with figure 6) while in the lower panel one can see the effect of the duration boundary shown in figure 4.

than $5M_\odot$ and mass ratio between 1 and 3 is the dense initially covered BBH region. The lack of templates just outside the stripe is due to the fact that templates at its boundary also cover systems just outside of it, such that the final covering step does not add templates there.

III. VALIDATION

In a matched-filter search, the maximum SNR that can be ideally observed for a given astrophysical signal (*optimal SNR*) requires a template that exactly matches the signal waveform. Because the template bank is discrete and finite and because the waveform model does not include the full physics of the system, the bank can only recover a fraction of the optimal SNR, which is known as the *fitting factor* φ between the signal and the bank [51]. Thus, given a population of N sources detectable with perfectly-matching templates, only αN source will be observed on average with a realistic bank, where $\alpha < 1$ is known as the *signal recovery fraction* [52] and is related to the fitting factor by

$$\alpha = \frac{\int \mathrm{d}\vec{x}\ \varphi^3(\vec{x})\sigma^3(\vec{x})}{\int \mathrm{d}\vec{x}\ \sigma^3(\vec{x})}. \tag{3}$$

Here $\vec{x}$ is the source's parameter vector (excluding the luminosity distance) and $\sigma(\vec{x})$ is the distance at which the optimal SNR of the source takes a fixed reference value[2]. Banks are typically constructed to achieve at least a 90% signal recovery fraction and it is customary to evaluate the correct performance of a bank in terms of fitting factor or signal recovery fraction. This can be done by simulating a large population of compact binary mergers at a fixed luminosity distance and calculating the fitting factor between each signal and the bank. Then the signal recovery fraction can be measured as

$$\alpha \approx \frac{\sum_i \varphi_i^3 \sigma_i^3}{\sum_i \sigma_i^3} \tag{4}$$

where i labels each simulated signal.

When testing a bank where all templates use the same lower cutoff frequency, the optimal SNR of each signal is calculated using the same cutoff. As such, the fitting factor only shows the SNR loss due to the discretization of the bank and any disagreement between the true signal and our waveform model. However, because templates in the bank described here have a variable f_{low}, optimal SNRs must now use a *lower* cutoff, which we choose to be fixed at 15 Hz, i.e. the reference frequency used for calculating each template's f_{low}. Therefore, our fitting factors also account for the fact that some SNR is lost due to a higher starting frequency of the templates. Since by our definition of f_{low} this loss is never smaller than 0.5%, our fitting factors cannot be larger than 99.5%.

We simulate three different classes of sources: BNS, NSBH and BBH. The BBH set is split into two subsets by $M = 100M_\odot$, where the lighter set is uniformly distributed in component masses and covers the BBH mass space used in O1, while the heavier set is distributed uniformly in M and mass ratio q and covers a mass range similar to the search space of [27]. Each set contains 5×10^4 systems and the parameters of the simulations can be found in table I. The waveform model used for the BNS simulations is the same post-Newtonian model used for templates with $M < 4M_\odot$; NSBH and BBH simulations use instead the same effective-one-body model used for templates with $M > 4M_\odot$. Note that the BBH simulations contain signals falling into the region excluded by the minimum-duration requirement, i.e. they span a slightly larger parameter space than the bank is designed to cover.

Figure 8 presents the signal recovery fractions and fitting factor distributions for each class. We divide the

[2] Normally taken to be 8, in which case the resulting σ is referred to as the *horizon distance*. However, the choice is arbitrary and does not change the value of the signal recovery fraction.

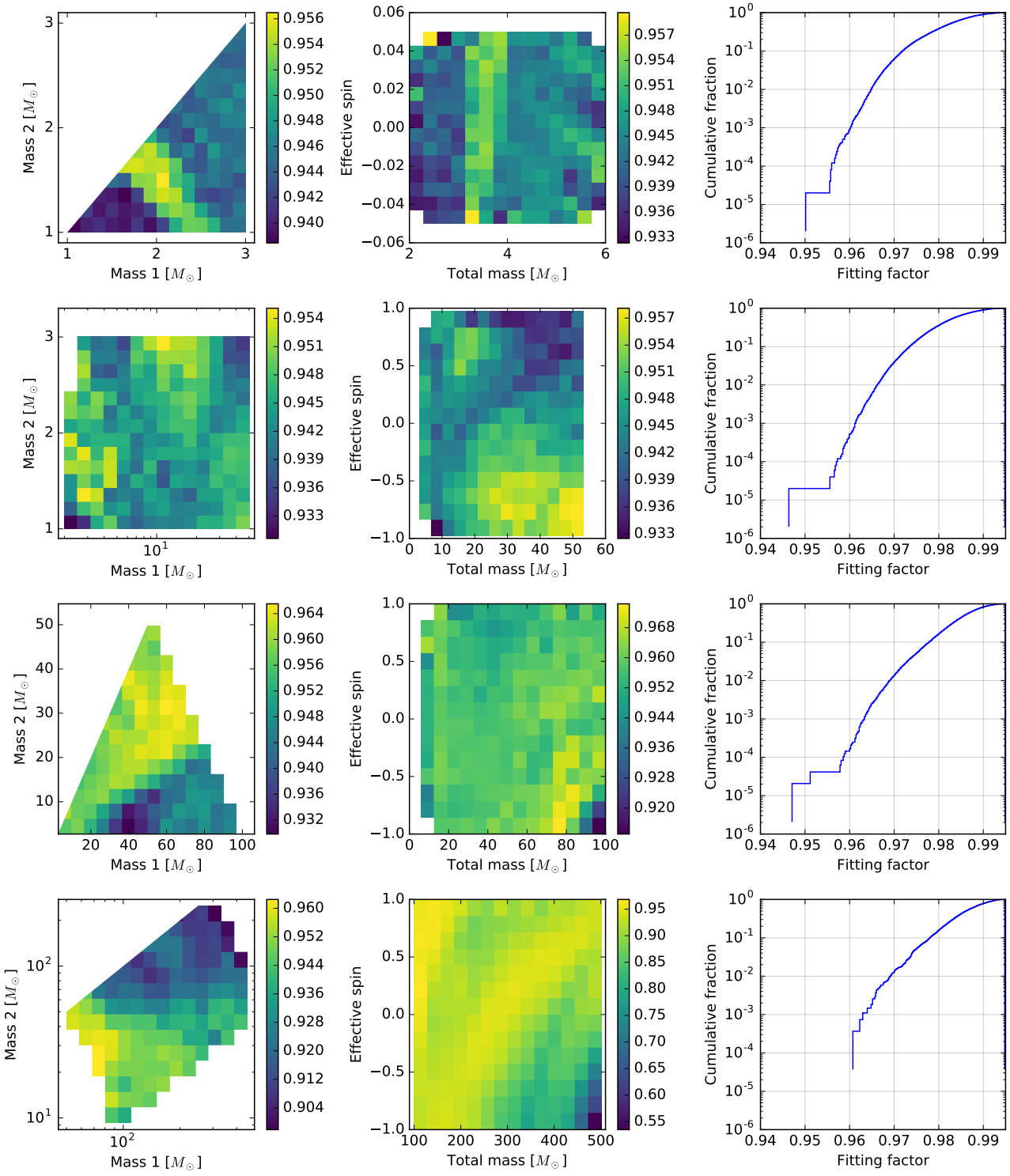

FIG. 8. Ability of the bank at detecting signals from BNS (top), NSBH (second row), BBH with $M < 100M_\odot$ (third row), and BBH with $M > 100M_\odot$ (bottom). The heat maps show the signal recovery fraction in each patch of parameter space. The cumulative distributions on the right show the fitting factors for signals strictly falling within the boundary of the search space. Signal recovery fractions are always larger than 90%, except for negatively-spinning, high-mass BBH systems, which the bank does not target. Only $\sim 1\%$ of the signals have an SNR loss larger than 3.5%. The loss is never smaller than 0.5% due to the choice of lower cutoff frequency of the templates.

Class	Masses ($M_\odot$)	Aligned spins	Waveform model
BNS	$m_{1,2} \in [1, 3]$	$\chi_{1,2} \in [\pm 0.05]$	Post-Newtonian
NSBH	$m_1 \in [2, 50]$ $m_2 \in [1, 3]$	$\chi_1 \in [\pm 1]$ $\chi_2 \in [\pm 0.05]$	Effective-one-body
BBH	$m_{1,2} > 3$ $M < 100$	$\chi_{1,2} \in [\pm 1]$	Effective-one-body
BBH	$M \in [100, 500]$ $q \in [1, 10]$	$\chi_{1,2} \in [\pm 1]$	Effective-one-body

TABLE I. Parameters of the simulated populations of compact binary mergers for testing the bank.

component-mass plane into bins and show the signal recovery fraction in each bin, to highlight possible systematic variations of the performance of the bank across the search space. The recovery fraction is larger than 90% in most bins, with the exception of BBH systems with $M \gtrsim 200 M_\odot$ and negative effective spins. Those cases, in fact, fall into the region excluded by the requirement on template duration. If we apply the same duration cut to exclude the simulated systems in that region, the resulting fitting factors are larger than 96.5% for 99% of the systems. Therefore, the bank meets the design expectations. It is also capable of observing a large fraction of systems immediately above its high-mass limit.

IV. CONCLUSION

In this work we present the motivation, novel methodology and resulting distribution of the template bank, which is currently being used by the `PyCBC` search for compact binary coalescences in Advanced LIGO's O2 data. The method described here creates a template bank covering a mass range that is as large as practically feasible with current waveform models, search techniques and detector performance.

In the future, it will be important to include even higher-mass BBH waveforms, improving the sensitivity to BBH systems heavier than the stellar-mass range and thus probing potentially different formation mechanisms than those producing stellar-mass BHs [53]. As the low-frequency sensitivity of Advanced LIGO proceeds towards the design target in the coming years, the duration boundary of the bank proposed here will automatically extend to include larger masses. It would also be useful to explore new search techniques for distinguishing more readily between noise transients and very short-duration compact binary merger signals, therefore lowering the minimum duration of the templates and raising the maximum mass even further. Highly-spinning effective-one-body waveforms were also found to be difficult to distinguish from certain noise artifacts and will require new methods before the maximum spin magnitude of the current bank can be safely brought to the Kerr limit.

There are also a number of physical effects that are currently ignored when creating this template bank. One important approximation is that the component spins are both restricted to be aligned with the direction of the orbital angular momentum. This scenario might be preferred if the compact binary is formed from an isolated stellar binary, but it is also possible that supernovae kicks can significantly misalign the component spins [54–56]. The compact bodies might also have formed separately in a dense environment, such as a globular cluster, and later formed a binary with randomly-oriented spins [57]. The impact of neglecting misaligned spins has been explored [41, 58, 59], and ideas for incorporating the effects of precessing spins have been suggested [52, 60]. Another current approximation is that radiation modes beyond the quadrupole are neglected in the search templates, and mostly impacts the sensitivity to asymmetric and high-mass compact binary mergers [61, 62]. Efforts are ongoing to extend the process described here and include these higher-order effects [63]. Orbital eccentricity, which presumably could be found in binaries formed in dense environments, is also currently neglected. While eccentric waveform models have been recently introduced [64–66], a full template bank has yet to be presented. Several waveform models also incorporate effects due to NS matter and its equation of state [67–70]. Whether and how to extend the current bank with such waveforms are currently open questions.

ACKNOWLEDGMENTS

We thank Alex Nitz, Tom Dent, Steve Privitera, Alex Nielsen, Alan Weinstein and Greg Mendell for useful discussion and comments. We are also grateful to Sarah Caudill for reading through the manuscript and providing thoughtful and helpful suggestions.

The authors thank the LIGO Scientific Collaboration for access to the data and gratefully acknowledge the support of the United States National Science Foundation (NSF) for the construction and operation of the LIGO Laboratory and Advanced LIGO as well as the Science and Technology Facilities Council (STFC) of the United Kingdom, and the Max-Planck-Society (MPS) for support of the construction of Advanced LIGO. Additional support for Advanced LIGO was provided by the Australian Research Council.

TDC was supported by an appointment to the NASA Postdoctoral Program at the Goddard Space Flight Center, administered by Universities Space Research Association under contract with NASA, during part of this work. IWH thanks the Max Planck Society for support.

Numerical computations and plots in this paper were performed with Python, NumPy [71] and Matplotlib [72] on the Atlas and Vulcan clusters of the Max Planck Institute for Gravitational Physics.

This paper has LIGO document number LIGO-

P1700085.

[1] G. M. Harry (LIGO Scientific), *Gravitational waves. Proceedings, 8th Edoardo Amaldi Conference, Amaldi 8, New York, USA, June 22-26, 2009*, Class. Quant. Grav. **27**, 084006 (2010).

[2] J. Aasi *et al.* (LIGO Scientific), Class. Quant. Grav. **32**, 074001 (2015), arXiv:1411.4547 [gr-qc].

[3] F. Acernese *et al.* (VIRGO), Class. Quant. Grav. **32**, 024001 (2015), arXiv:1408.3978 [gr-qc].

[4] K. Somiya (KAGRA), *Gravitational waves. Numerical relativity - data analysis. Proceedings, 9th Edoardo Amaldi Conference, Amaldi 9, and meeting, NRDA 2011, Cardiff, UK, July 10-15, 2011*, Class. Quant. Grav. **29**, 124007 (2012), arXiv:1111.7185 [gr-qc].

[5] Y. Aso, Y. Michimura, K. Somiya, M. Ando, O. Miyakawa, T. Sekiguchi, D. Tatsumi, and H. Yamamoto (KAGRA), Phys. Rev. **D88**, 043007 (2013), arXiv:1306.6747 [gr-qc].

[6] B. P. Abbott *et al.* (Virgo, LIGO Scientific), Phys. Rev. Lett. **116**, 061102 (2016), arXiv:1602.03837 [gr-qc].

[7] B. P. Abbott *et al.* (Virgo, LIGO Scientific), Phys. Rev. Lett. **116**, 241103 (2016), arXiv:1606.04855 [gr-qc].

[8] B. P. Abbott *et al.* (Virgo, LIGO Scientific), Phys. Rev. X **6**, 041015 (2016), arXiv:1606.04856 [gr-qc].

[9] B. S. Sathyaprakash and S. V. Dhurandhar, Phys. Rev. **D44**, 3819 (1991).

[10] B. J. Owen, Phys. Rev. D **53**, 6749 (1996).

[11] B. J. Owen and B. S. Sathyaprakash, Phys. Rev. D **60**, 022002 (1999).

[12] T. Cokelaer, Phys. Rev. D **76**, 102004 (2007).

[13] R. Prix, Classical and Quantum Gravity **24**, S481 (2007), arXiv:0707.0428 [gr-qc].

[14] I. W. Harry, B. Allen, and B. S. Sathyaprakash, Phys. Rev. D **80**, 104014 (2009).

[15] P. Ajith, N. Fotopoulos, S. Privitera, A. Neunzert, N. Mazumder, and A. J. Weinstein, Phys. Rev. D **89**, 084041 (2014).

[16] B. Allen, W. G. Anderson, P. R. Brady, D. A. Brown, and J. D. E. Creighton, Phys. Rev. D **85**, 122006 (2012), arXiv:gr-qc/0509116 [gr-qc].

[17] T. Dal Canton, A. H. Nitz, A. P. Lundgren, A. B. Nielsen, *et al.*, Phys. Rev. D **90**, 082004 (2014), arXiv:1405.6731 [gr-qc].

[18] S. A. Usman *et al.*, Class. Quant. Grav. **33**, 215004 (2016), arXiv:1508.02357 [gr-qc].

[19] A. H. Nitz, I. Harry, C. M. Biwer, D. A. Brown, J. Willis, T. D. Canton, L. Pekowsky, T. Dent, A. R. Williamson, C. Capano, S. De, P. Kumar, B. Machenschalk, M. Cabero, T. Massinger, A. Lenon, S. Fairhurst, S. Reyes, A. Nielsen, S. Kapadia, F. Pannarale, L. Singer, S. Babak, D. Macleod, C. Sugar, L. M. na Zertuche, J. Veitch, P. Couvares, B. Bockelman, and N. W. Brown, "Pycbc software," (2017).

[20] A. Nitz, T. Dent, T. Dal Canton, S. Fairhurst, and D. Brown, (2017).

[21] K. Cannon *et al.*, Astrophys. J. **748**, 136 (2012), arXiv:1107.2665 [astro-ph.IM].

[22] S. Privitera, S. R. P. Mohapatra, P. Ajith, K. Cannon, N. Fotopoulos, M. A. Frei, C. Hanna, A. J. Weinstein, and J. T. Whelan, Phys. Rev. **D89**, 024003 (2014), arXiv:1310.5633 [gr-qc].

[23] C. Messick *et al.*, Phys. Rev. **D95**, 042001 (2017), arXiv:1604.04324 [astro-ph.IM].

[24] T. Adams, D. Buskulic, V. Germain, G. M. Guidi, F. Marion, M. Montani, B. Mours, F. Piergiovanni, and G. Wang, Class. Quant. Grav. **33**, 175012 (2016), arXiv:1512.02864 [gr-qc].

[25] D. Keppel, Phys. Rev. **D87**, 124003 (2013), arXiv:1303.2005 [physics.data-an].

[26] B. P. Abbott *et al.* (Virgo, LIGO Scientific), Astrophys. J. **832**, L21 (2016), arXiv:1607.07456 [astro-ph.HE].

[27] B. P. Abbott *et al.* (LIGO Scientific Collaboration, Virgo collaboration), (2017), arXiv:1704.04628 [gr-qc].

[28] R. Biswas *et al.*, Phys. Rev. **D85**, 122009 (2012), arXiv:1201.2964 [gr-qc].

[29] D. Keppel, (2013), arXiv:1307.4158 [gr-qc].

[30] M. Pürrer, Class. Quant. Grav. **31**, 195010 (2014), arXiv:1402.4146 [gr-qc].

[31] A. Taracchini *et al.*, Phys. Rev. **D89**, 061502 (2014), arXiv:1311.2544 [gr-qc].

[32] A. Buonanno, B. Iyer, E. Ochsner, Y. Pan, and B. S. Sathyaprakash, Phys. Rev. **D80**, 084043 (2009), arXiv:0907.0700 [gr-qc].

[33] K. G. Arun, A. Buonanno, G. Faye, and E. Ochsner, Phys. Rev. **D79**, 104023 (2009), [Erratum: Phys. Rev.D84,049901(2011)], arXiv:0810.5336 [gr-qc].

[34] A. Bohé, L. Shao, A. Taracchini, A. Buonanno, S. Babak, I. W. Harry, I. Hinder, S. Ossokine, M. Pürrer, V. Raymond, T. Chu, H. Fong, P. Kumar, H. P. Pfeiffer, M. Boyle, D. A. Hemberger, L. E. Kidder, G. Lovelace, M. A. Scheel, and B. Szilágyi, Phys. Rev. D **95**, 044028 (2017).

[35] A. Bohé, S. Marsat, and L. Blanchet, Class. Quant. Grav. **30**, 135009 (2013), arXiv:1303.7412 [gr-qc].

[36] "The LIGO algorithms library," `https://www.lsc-group.phys.uwm.edu/daswg/projects/lalsuite.html`.

[37] M. C. Miller and J. M. Miller, Phys.Rept. **548**, 1 (2014), arXiv:1408.4145 [astro-ph.HE].

[38] A. Nitz, Ph.D. thesis, Syracuse University (2015).

[39] D. R. Lorimer, Living Rev. Rel. **11**, 8 (2008), arXiv:0811.0762 [astro-ph].

[40] J. E. McClintock, R. Narayan, and J. F. Steiner, (2013), arXiv:1303.1583 [astro-ph.HE].

[41] B. P. Abbott *et al.* (Virgo, LIGO Scientific), Phys. Rev. D **93**, 122003 (2016), arXiv:1602.03839 [gr-qc].

[42] S. Klimenko *et al.*, Phys. Rev. **D93**, 042004 (2016), arXiv:1511.05999 [gr-qc].

[43] B. S. Sathyaprakash, Phys. Rev. D **50**, R7111 (1994).

[44] M. Pürrer, Phys. Rev. **D93**, 064041 (2016), arXiv:1512.02248 [gr-qc].

[45] S. E. Gralla, S. A. Hughes, and N. Warburton, Class. Quant. Grav. **33**, 155002 (2016), arXiv:1603.01221 [gr-qc].

[46] B. Allen, Phys. Rev. D **71**, 062001 (2005), arXiv:gr-qc/0405045 [gr-qc].

[47] S. Babak, R. Biswas, P. R. Brady, D. A. Brown, *et al.*,

Phys. Rev. D **87**, 024033 (2013).
[48] B. P. Abbott *et al.* (LIGO Scientific Collaboration), Phys. Rev. D **95**, 062003 (2017).
[49] T. Dal Canton, S. Bhagwat, S. V. Dhurandhar, and A. Lundgren, Classical and Quantum Gravity **31**, 015016 (2014), arXiv:1304.0008 [gr-qc].
[50] C. Capano, I. Harry, S. Privitera, and A. Buonanno, Phys. Rev. D **93**, 124007 (2016), arXiv:1602.03509 [gr-qc].
[51] T. A. Apostolatos, Phys. Rev. D **52**, 605 (1995).
[52] I. Harry, S. Privitera, A. Bohé, and A. Buonanno, Phys. Rev. **D94**, 024012 (2016), arXiv:1603.02444 [gr-qc].
[53] M. C. Miller and E. J. M. Colbert, Int. J. Mod. Phys. **D13**, 1 (2004), arXiv:astro-ph/0308402 [astro-ph].
[54] V. Kalogera, Astrophys.J. **541**, 319 (2000), arXiv:astro-ph/9911417 [astro-ph].
[55] D. Gerosa, M. Kesden, E. Berti, R. O'Shaughnessy, and U. Sperhake, Phys. Rev. **D87**, 104028 (2013), arXiv:1302.4442 [gr-qc].
[56] W. M. Farr, K. Kremer, M. Lyutikov, and V. Kalogera, The Astrophysical Journal **742**, 81 (2011).
[57] C. L. Rodriguez, M. Zevin, C. Pankow, V. Kalogera, and F. A. Rasio, Astrophys. J. **832**, L2 (2016), arXiv:1609.05916 [astro-ph.HE].
[58] D. A. Brown, A. Lundgren, and R. O'Shaughnessy, Phys. Rev. D **86**, 064020 (2012), arXiv:1203.6060 [gr-qc].
[59] T. Dal Canton, A. P. Lundgren, and A. B. Nielsen, Phys. Rev. D **91**, 062010 (2015), arXiv:1411.6815 [gr-qc].
[60] N. Indik, K. Haris, T. Dal Canton, H. Fehrmann, B. Krishnan, A. Lundgren, A. B. Nielsen, and A. Pai, (2016), arXiv:1612.05173 [gr-qc].
[61] V. Varma, P. Ajith, S. Husa, J. C. Bustillo, M. Hannam, and M. Pürrer, Phys. Rev. **D90**, 124004 (2014), arXiv:1409.2349 [gr-qc].
[62] J. Calderón Bustillo, P. Laguna, and D. Shoemaker, (2016), arXiv:1612.02340 [gr-qc].
[63] C. Capano, Y. Pan, and A. Buonanno, Phys. Rev. **D89**, 102003 (2014), arXiv:1311.1286 [gr-qc].
[64] B. Moore, M. Favata, K. G. Arun, and C. K. Mishra, Phys. Rev. **D93**, 124061 (2016), arXiv:1605.00304 [gr-qc].
[65] S. Tanay, M. Haney, and A. Gopakumar, Phys. Rev. **D93**, 064031 (2016), arXiv:1602.03081 [gr-qc].
[66] E. A. Huerta *et al.*, Phys. Rev. **D95**, 024038 (2017), arXiv:1609.05933 [gr-qc].
[67] K. Hotokezaka, K. Kyutoku, H. Okawa, M. Shibata, and K. Kiuchi, Phys. Rev. D **83**, 124008 (2011).
[68] F. Pannarale, E. Berti, K. Kyutoku, and M. Shibata, Phys. Rev. D **88**, 084011 (2013).
[69] B. D. Lackey, K. Kyutoku, M. Shibata, P. R. Brady, and J. L. Friedman, Phys. Rev. D **89**, 043009 (2014).
[70] F. Pannarale, E. Berti, K. Kyutoku, B. D. Lackey, and M. Shibata, Phys. Rev. **D92**, 084050 (2015), arXiv:1509.00512 [gr-qc].
[71] S. van der Walt, S. C. Colbert, and G. Varoquaux, Computing in Science & Engineering **13**, 22 (2011).
[72] J. D. Hunter, Computing In Science & Engineering **9**, 90 (2007).